

# 1 **High-Capacity Reversible Lithium Storage in Defined Microporous Carbon** 2 **Framework for All Solid-State Lithium Batteries**

3  
4 Luise Maria Bloi<sup>a,b</sup>, Felix Hippauf<sup>b</sup>, Tom Boenke<sup>a,b</sup>, Marcus Rauche<sup>c</sup>, Silvia Paasch<sup>c</sup>, Konstantin  
5 Schutjajew<sup>d,e</sup>, Jonas Pampel<sup>d</sup>, Friedrich Schwotzer<sup>a</sup>, Susanne Dörfler<sup>b</sup>, Holger Althues<sup>b</sup>, Martin  
6 Oschatz<sup>d,e</sup>, Eike Brunner<sup>c</sup>, Stefan Kaskel<sup>a,b\*</sup>

## 7 8 9 **Abstract**

10 For decades graphite has been used as the anode material of choice for lithium batteries since porous  
11 carbons were believed to be inappropriate because of their high potential slope during lithiation as well  
12 as capacity losses due to intense formation of solid electrolyte interphase (SEI).

13 However, in this work we demonstrate a microporous carbide-derived carbon material (HCmicro) to  
14 provide a high-capacity anode framework for lithium storage in all solid-state batteries. Half-cell  
15 measurements of HCmicro exhibit exceptionally high and reversible lithiation capacities of  
16 1000 mAh g<sup>-1</sup><sub>carbon</sub> utilizing an extremely long voltage plateau near 0 V vs. Li/Li<sup>+</sup>. The defined  
17 microporosity of the HCmicro combined well with the argyrodite-type electrolyte (Li<sub>6</sub>PS<sub>5</sub>Cl)  
18 suppressing extensive SEI formation to deliver high coulombic efficiencies. Preliminary full-cell  
19 measurements vs. NMC-cathodes (LiNi<sub>0.9</sub>Co<sub>0.05</sub>Mn<sub>0.05</sub>O<sub>2</sub>) obtained a considerably improved average  
20 potential of 3.76 V leading to a projected energy density as high as 443 Wh kg<sup>-1</sup>. <sup>7</sup>Li Nuclear Magnetic  
21 Resonance spectroscopy was combined with ex-situ Small Angle X-ray Scattering and further  
22 electrochemical investigations to elucidate the storage mechanism of lithium inside the carbon matrix  
23 revealing the formation of extended quasi-metallic lithium clusters.

## 24 25 **Introduction**

26 The development of batteries for consumer electronics continually advances volumetric and gravimetric  
27 energy density leading to smaller and lighter devices. For electric vehicles, longer range and higher  
28 energy density are desired. Lithium metal anodes are attractive candidates to fulfil these goals, owing to  
29 their high theoretical specific capacity of 3860 mAh g<sup>-1</sup> and low voltage of -3.04 V vs. SHE. However,  
30 due to the high reactivity of lithium metal causing dendrite formation and electrolyte decomposition,  
31 long-term cycling remains problematic under practical conditions.<sup>1-4</sup> Stable negative electrodes like  
32 commercial graphite, on the other hand, suffer from low theoretical specific capacity with only little  
33 opportunity for further optimization. The ideal anode material therefore combines the high gravimetric  
34 capacity of a lithium metal anode with the cycle stability of a graphite anode, gaining long-life batteries  
35 with high energy density.

1 Over the last decades, progress has been made in increasing the lithiation capacity of carbon materials.  
2 Several hard carbons (HC) or micro- and mesoporous carbons have been presented exceeding the  
3 theoretical capacity of graphite of  $372 \text{ mAh g}^{-1}$ . Some of them show high specific capacities of  
4  $1500 \text{ mAh g}^{-1}$  or even beyond in the 1<sup>st</sup> lithiation.<sup>5-8</sup> However, most of them suffer from limited  
5 reversible capacity and usually exhibit a very long so-called sloping region in their voltage profiles,  
6 which considerably lowers the resulting full-cell voltage.

7 Increasing anode capacity at a lower voltage plateau requires the formation of metallic lithium though,  
8 which needs to be stabilized for reversible cycling. By adapting the liquid electrolyte and additives or  
9 by applying pressure, the long-term stability of lithium-metal batteries could be increased as just recently  
10 reported by Dahn et al.<sup>9,10</sup> However, especially at room temperature, plating and stripping of lithium is  
11 limited to certain current densities and capacities.<sup>11</sup> When leaving the narrow range of suitable  
12 parameters, dendrite formation and porous lithium growth occur as reviewed e.g. by Zhang et al.<sup>4,12</sup> By  
13 directing lithium deposition, e.g., using a porous host matrix, a defined interface can be formed that  
14 inhibits side reactions with the electrolyte and the effective current density is reduced leading to an  
15 enhanced cycle life.<sup>13-17</sup>

16 A porous carbon material is a good choice as anode material due to its low weight, tunable pore  
17 architecture and good electric conductivity. The microporous structure is able to stabilize molecules or  
18 metal clusters by decreasing their chemical potential.<sup>18-20</sup> Hence, pores potentially act as seeding sites  
19 directing lithium deposition preferentially towards the pore interior. The formation of lithium quasi-  
20 metallic clusters – microscopic aggregates consisting of a few tens through a few hundreds of lithium  
21 atoms<sup>21</sup> – in the inner porosity of HCs was detected by Tatsumi et al. by <sup>7</sup>Li nuclear magnetic resonance  
22 (NMR) measurements.<sup>22</sup> Cluster formation is one possibility to store excess lithium at low potentials vs.  
23 Li/Li<sup>+</sup>. Only recently, an operando <sup>7</sup>Li NMR study on HC and graphite half-cells has been published by  
24 Gotoh et al. investigating overlithiation behavior of the lithium NMR signal in different carbon  
25 materials.<sup>23</sup>

26 We envisioned carbide-derived carbons (CDCs) to offer an ideal microporous carbon framework for  
27 stabilizing lithium clusters due to their narrow pore size distribution, which can be precisely tuned.<sup>24-27</sup>  
28 However, their high porosity comprises pores that are accessible for small molecules like N<sub>2</sub> or liquid  
29 electrolyte components as well as defect sites in the hexagonal carbon structure. In combination with  
30 the electronic conductivity of the carbon, both tend to deplete liquid electrolytes and promote solid  
31 electrolyte interphase (SEI) formation leading to irreversible lithium and capacity losses.<sup>8,15</sup>

32

33 In the following we demonstrate the application of a defined microporous carbide-derived carbon  
34 (TiC-CDC,<sup>28</sup> further named as HCmicro) as a carbon/lithium hybrid anode within an all solid-state  
35 battery (ASSB) set-up that tackles these challenges and reveals clear advantage compared with a  
36 commercial hard carbon (HC). Unlike solvent-based electrolytes, the solid electrolyte cannot penetrate  
37 the accessible porosity of the framework, which is why this system suppresses extensive SEI formation

1 on accessible micropores, and thus, leads to reduced capacity loss in the first cycles as well as long-term  
2 stabilization of lithium deposited inside the pores. Half-cell measurements of HCmicro exhibit  
3 exceptionally high and reversible lithiation capacities of up to 1000 mAh g<sup>-1</sup><sub>carbon</sub> utilizing an extremely  
4 long voltage plateau region near 0 V vs. Li/Li<sup>+</sup>. Even at room temperature, no short circuit due to  
5 dendrite formation is observed. With the solid electrolyte the herein presented system comprises a  
6 remarkably high coulombic efficiency (CE) of 70% in the 1<sup>st</sup> cycle in comparison with other battery  
7 systems utilizing accessible microporous carbon materials, which usually have an initial CE in the range  
8 of 30 to 50%.<sup>5,6</sup> Via magic angle spinning (MAS) <sup>7</sup>Li NMR measurements we demonstrate the lithiation  
9 mechanism to rely on lithium cluster formation inside the pores with special features for the HCmicro-  
10 electrode. The latter, to the best of our knowledge have not been observed for lithiated carbon electrodes  
11 so far.<sup>22,23,29-34</sup> Based on these findings, we propose a lithiation mechanism of HCmicro in the all solid-  
12 state system via the reversible formation of extended lithium clusters in the carbon framework.

13

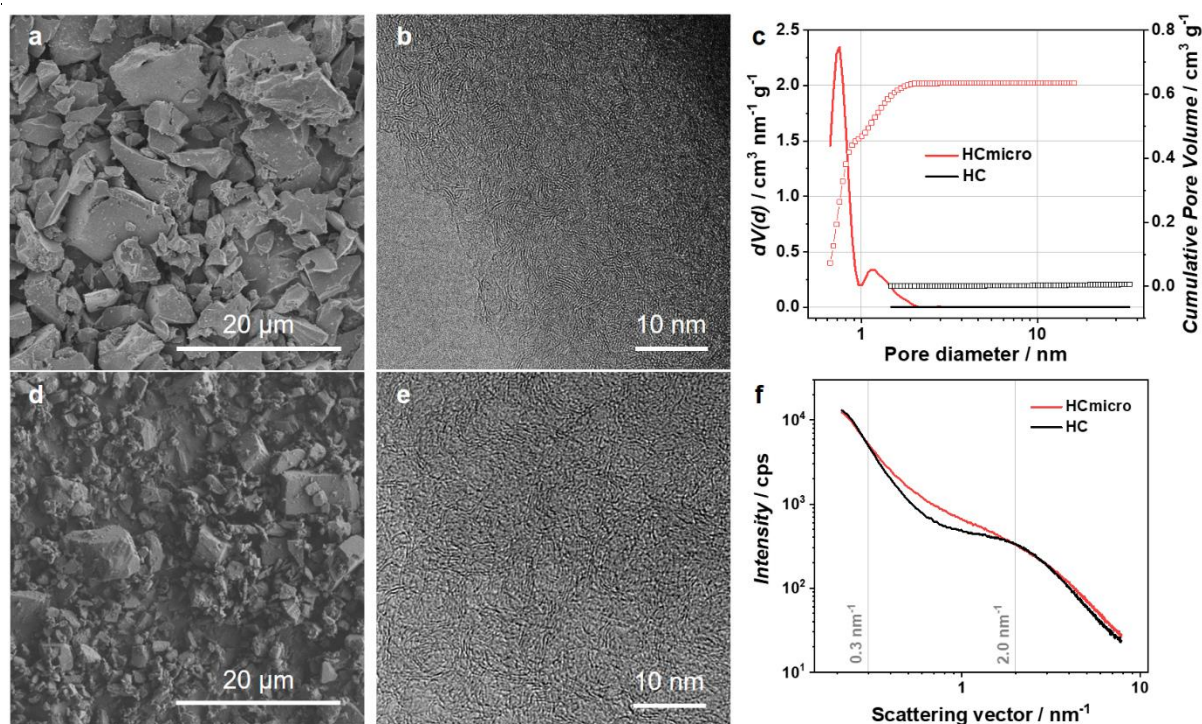
14

### 15 **Structural and morphological characteristics of the porous carbon structure**

16 The microporous carbon HCmicro and the commercial HC chosen as reference were initially  
17 investigated with regard to their structural and morphological features (Figure 1). Scanning electron  
18 microscopy (SEM) and transmission electron microscopy (TEM) revealed the differences of both  
19 carbons in terms of carbon nanostructure and particle size. SEM images display particle diameters of  
20 around 10 μm for the HC compared to 5 μm for HCmicro while both samples also contain much smaller  
21 particles in the range of 1 μm and below. Both carbons show irregular shaped particles with sharp edges.  
22 The TEM images depict differences in size and shape of graphite-like domains between HCmicro and  
23 HC. These domains show random turbostratic orientation for both carbons with shortened average lateral  
24 length of the parallel graphite-like segments for the HCmicro as well as decreased average curvature  
25 radius in comparison with the HC. HCmicro additionally comprises a lower average number of parallel  
26 stacked graphene sheets overall showing good agreement with literature results for both carbon  
27 materials.<sup>35,36</sup>

28 Nitrogen physisorption analysis at 77 K results in a type I isotherm for HCmicro (Supplementary  
29 Figure 1) typical for microporous materials but no accessible porosity for the HC with a type II isotherm  
30 characteristic for non-porous materials (according to the IUPAC classification<sup>37</sup>). The specific BET  
31 surface area and total pore volume are 1520 m<sup>2</sup> g<sup>-1</sup> and 0.63 cm<sup>3</sup> g<sup>-1</sup> for HCmicro and 3.8 m<sup>2</sup> g<sup>-1</sup> and  
32 0.006 cm<sup>3</sup> g<sup>-1</sup> for HC, respectively. The pore size distributions of both carbons were determined via  
33 quenched-solid density functional theory (QSDFT) calculations (Figure 1c). The main pore diameter in  
34 HCmicro is 0.75 nm with 75% of its total pore volume reached at diameters up to 1 nm. Larger micro-  
35 and small mesopores until the diameter of 3 nm contribute further. The HC, in comparison, comprises  
36 nearly no accessible porosity for N<sub>2</sub> molecules resulting in a very low cumulative pore volume.

1 As established hard carbons are known to have closed intrinsic porosity, which means pore volume that  
 2 is present within the material but remains inaccessible in gas physisorption for nitrogen as the probe gas  
 3 at 77 K. Therefore, we measured Small Angle X-ray Scattering (SAXS) (Figure 1f) to investigate further  
 4 the porosity of both materials.<sup>38</sup> Both SAXS measurements exhibit scattering curves with comparable  
 5 intensities at scattering vectors ( $Q$ ) above  $2 \text{ nm}^{-1}$  and below  $0.3 \text{ nm}^{-1}$ . The respective regions are mainly  
 6 influenced by the scattering of the macroscopic particle surface area for small values of  $Q$  and the  
 7 scattering on micropores for high  $Q$  values.<sup>39</sup> In the scattering region between  $2 \text{ nm}^{-1}$  and  $0.3 \text{ nm}^{-1}$ , a  
 8 flattened sloping with higher scattering intensity is observed for HCmicro. According to Saurel et al.  
 9 pore-pore connections occurring from fractal aggregates of pores lead to an increased contribution of  
 10 the scattering between  $Q$  values corresponding to micropore and particle scattering.<sup>39</sup> This is due to the  
 11 dimension of the fractal pore-pore connections. Such aggregates can be attributed to an accessible pore  
 12 structure such as of HCmicro resulting in a higher scattering intensity and flattened slope in this region  
 13 as observed in the SAXS curves. However, both curves show comparable intensities above  $2 \text{ nm}^{-1}$   
 14 revealing the existence of microporosity for both carbons that differs mainly in inter-pore connectivity.  
 15  
 16



17  
 18 **Figure 1: Characterization of the carbon materials.** SEM and TEM images of HC (a and b,  
 19 respectively) and HCmicro (d and e, respectively). Pore size distribution and cumulative pore volume  
 20 (c) obtained from  $\text{N}_2$  physisorption measurements at 77 K (Supplementary Figure 1) and SAXS data (f)  
 21 for both carbons (red: HCmicro; black: HC).  
 22

23 Further investigations via powder X-Ray Diffraction (PXRD) and Raman measurements are visualized  
 24 and discussed in the supplementary material (Supplementary Figure 1). In summary, the materials are  
 25 of comparable morphology and structure with probably slightly lower amount and size of graphite-like

1 domains for HCmicro. Both carbons possess porosity predominantly in the microporous range, however,  
2 with different pore accessibility for N<sub>2</sub> molecules. This leads to the differentiation into “open porous  
3 system” for the HCmicro and “closed porous system” for the HC.

#### 6 **Calculation of maximum lithiation capacity for HCmicro**

7 Aurbach et al. proposed a possible lithiation capacity of 1400 mAh g<sup>-1</sup> for an activated microporous  
8 carbon protected against electrolyte penetration by a pyrolytic carbon layer. They calculated the  
9 theoretical maximum lithiation capacity based on the complete filling of the microporosity with lithium  
10 metal. Practically, however, they have been able to gain only about 10% of this value due to incomplete  
11 pore coverage leading to continuous SEI formation during lithium deposition.<sup>15</sup> Our approach therefore  
12 employs a solid electrolyte to avoid pore penetration by liquid and supersede any additional carbon  
13 coverage e.g. to minimize weight of inactive material.

14 For calculation of the theoretical maximum of lithium-storage capacity of the herein used HCmicro, we  
15 assumed the accessible total pore volume obtained from N<sub>2</sub>-physisorption (0.63 cm<sup>3</sup> g<sup>-1</sup><sub>HCmicro</sub>) as  
16 accessible void for lithium insertion.<sup>15</sup> Assuming that the density of lithium stored in pores is similar to  
17 the bulk density of lithium (0.534 g<sub>Li</sub> cm<sup>-3</sup>), we can estimate the amount of storable lithium in the open  
18 pore structure of HCmicro (0.336 g<sub>Li</sub> g<sup>-1</sup><sub>HCmicro</sub> or 1300 mAh g<sup>-1</sup>). Compared to reversible lithiation  
19 capacities of different HCs with a maximum of 550 mAh g<sup>-1</sup><sub>HC</sub> in liquid electrolytes<sup>7</sup> this corresponds  
20 to an almost two and a half times higher reversible capacity.

21 For the definition of the testing parameters, irreversible capacity resulting from side reactions and an  
22 incomplete pore filling due to geometric restrictions need to be considered. Hence, for the test protocol  
23 in this work, a constant lithiation capacity of 1000 mAh g<sup>-1</sup><sub>carbon</sub> was applied to compare the HCmicro  
24 with the commercial HC.

#### 27 **Electrochemical evaluation in half-cells vs. lithium metal**

28 For electrochemical evaluation of the materials in ASSBs, the carbons were prepared as powder  
29 electrodes via blending the carbon with solid electrolyte (SE) and a conducting additive in a weight ratio  
30 of 60:35:5. The resulting batch powders are denoted as “*active material-electrode*” (graphite-electrode,  
31 HC-electrode and HCmicro-electrode) to differentiate from the pure carbon powder. Firstly, the  
32 HCmicro-electrode and HC-electrode were evaluated against lithium metal foil. The resulting  
33 electrochemical cell is named a “half-cell” due to evaluation of only one electrode (in this case the  
34 carbon anode) of the intended battery cell that is then called a “full-cell”. All stated potential values in  
35 this section are therefore measured vs. Li/Li<sup>+</sup> and shall be read as V or mV “vs. Li/Li<sup>+</sup>” though this  
36 phrase is not especially written for each individual case. The half-cells were electrochemically evaluated  
37 in 10 cycles of lithiation of the carbon anode by discharging with 0.05 mA cm<sup>-2</sup> up to 1000 mAh g<sup>-1</sup><sub>carbon</sub>

1 and subsequent charging/delithiation at the same current density until the voltage limit of 2 V was  
2 reached (Figure 2).

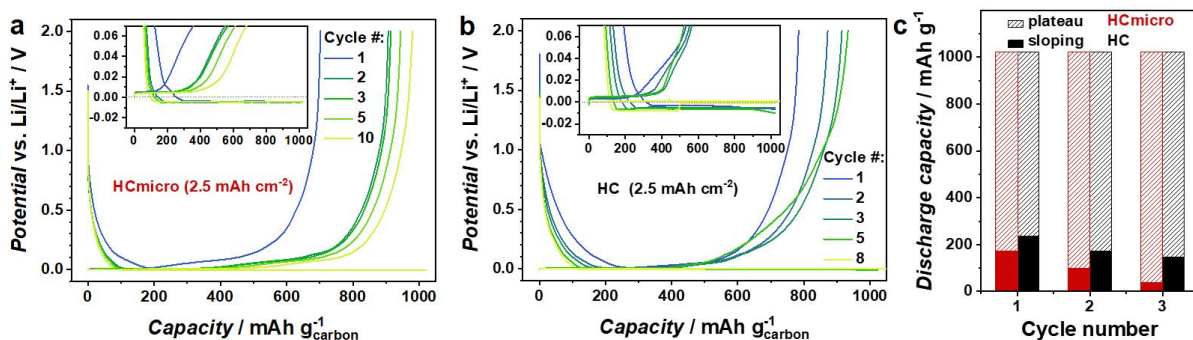
3 The resulting voltage profiles for the lithiation of the HCmicro-electrode (Figure 2a) show a short and  
4 steep voltage decrease followed by a long plateau below 20 mV. This plateau starts at 172 mAh g<sup>-1</sup><sub>HCmicro</sub>  
5 in the 1<sup>st</sup> cycle and stays above -5.5 mV until the end of lithiation at 1000 mAh g<sup>-1</sup> for all 10 cycles (see  
6 inset). It is noteworthy that the voltage profiles do not comprise a nucleation dip at the beginning of the  
7 plateau region. This temporary decrease in cell potential is associated with overcoming the overpotential  
8 for the nucleation of lithium metal on a substrates surface and is therefore assigned to the start of lithium  
9 metal plating.<sup>23</sup> The delithiation of the HCmicro-electrode exhibits a very long plateau region close to  
10 0 V divided into two parts before the voltage increases sharply at the end of delithiation. During the first  
11 delithiation, the first plateau (up to 20 mV) contributes to 210 mAh g<sup>-1</sup><sub>HCmicro</sub> and the second plateau  
12 (above 20 mV) adds another 332 mAh g<sup>-1</sup><sub>HCmicro</sub> until the voltage reaches 0.2 V. In total, the plateau  
13 capacity reaches 542 mAh g<sup>-1</sup><sub>HCmicro</sub> in the 1<sup>st</sup> and 827 mAh g<sup>-1</sup><sub>HCmicro</sub> in the 10<sup>th</sup> cycle. Generally, minor  
14 capacity values are obtained in the sloping region above 0.2 V, i.a. due to the nature of the solid  
15 electrolyte not being able to form an electrochemical double layer.

16 The HC-electrode half-cell (Figure 2b) shows a different behaviour in the 1<sup>st</sup> cycle. The discharge  
17 voltage curve falls below -5.5 mV after a capacity of 880 mAh g<sup>-1</sup><sub>HC</sub> and continues to decrease. In further  
18 discharge cycles, the cell voltage crosses -5.5 mV shortly after the end of the sloping region forming a  
19 slight dip. In the 8<sup>th</sup> cycle, the voltage signal experiences a sharp rise to 0 V after merely 495 mAh g<sup>-1</sup><sub>HC</sub>  
20 of lithiation indicating the formation of a dendrite. Consequently, the cell cannot reach the upper cut-off  
21 voltage in the subsequent charging step. However, the 1<sup>st</sup> charging profile of the HC half-cell still shows  
22 a plateau capacity of 338 mAh g<sup>-1</sup><sub>HC</sub> up to 20 mV, corresponding to an increase of ca. 60% when  
23 compared to the HCmicro-electrode. The second plateau until 0.2 V exhibits a capacity of  
24 282 mAh g<sup>-1</sup><sub>HC</sub> and is therefore shortened in comparison to the HCmicro-electrode (total plateau  
25 capacity of 620 mAh g<sup>-1</sup><sub>HC</sub>).

26 The two plateaus formed in delithiation of the carbons indicate the existence of two different delithiation  
27 mechanisms occurring in both carbons to different extent. The plateau up to 20 mV can be attributed to  
28 the stripping of metallic lithium from a 3D structured conducting material due to the small hysteresis  
29 between plating and stripping in the case of low current densities (0.05 mA cm<sup>-2</sup>).<sup>40</sup> The other  
30 delithiation plateau between 20 mV and 0.2 V cannot be assigned to a certain species at this point.

31





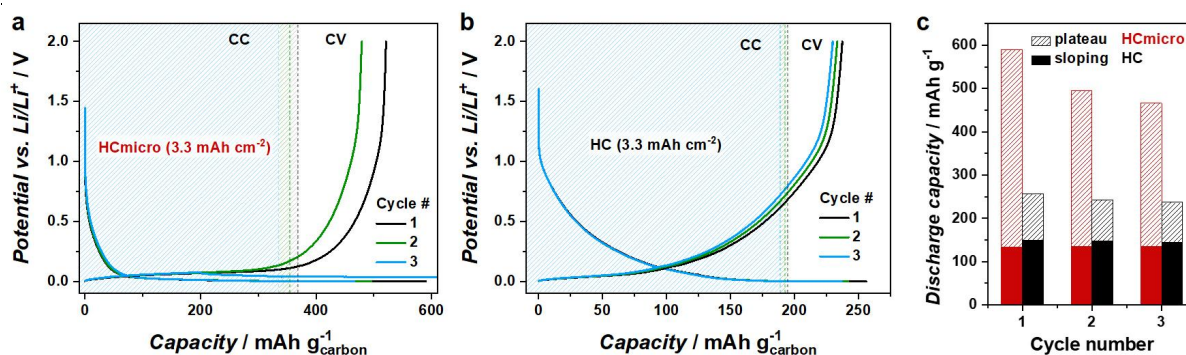
1  
2 **Figure 2: Electrochemical characterization via constant current (CC) measurement.** Voltage  
3 profiles of HCmicro (a) and HC (b) half-cells vs. lithium metal galvanostatically cycled at  $0.05 \text{ mA cm}^{-2}$   
4 between 2 V and a constant capacity of  $1000 \text{ mAh g}^{-1}_{\text{carbon}}$  in discharge with an areal loading of  
5  $2.5 \text{ mAh cm}^{-2}$ . (c) Comparison of sloping (until 20 mV, filled area) and plateau discharge capacities  
6 (below 20 mV, hatched area) for both carbon half-cells in the first 3 cycles.

7  
8 The HCmicro half-cell reaches slightly lower initial CE (70%) than the HC half-cell (77%) but improves  
9 rapidly to 98% CE with a delithiation capacity of  $980 \text{ mAh g}^{-1}_{\text{HCmicro}}$  in the 10<sup>th</sup> cycle. In contrast, the  
10 HC half-cell fails in 8<sup>th</sup> lithiation due to micro short-circuit of the cell. The shown example for a HC  
11 half-cell, however, is no outlier. We tested various HC half-cells each failing due to short-circuit within  
12 their first 8 cycles while HCmicro half-cells did not show this phenomenon. Despite the fact that no  
13 liquid electrolyte penetrates the pores, the lower initial CE is not unusual for a porous carbon with a  
14 high specific surface area, since, e.g., lithium can react with carbon dangling bonds at the carbon surface.  
15 In the following cycles, the CE for HCmicro half-cell show remarkably high values compared to other  
16 carbon electrodes with N<sub>2</sub>-accessible porosity stated in literature.<sup>5,6,41</sup> The application of HCmicro in  
17 liquid electrolyte systems cannot compete with the herein stated all solid-state system in terms of CEs  
18 and delithiation capacities.<sup>8,28</sup> This indicates that the combination of the open porous HCmicro with the  
19 solid electrolyte prevents penetration of electrolyte components into the microporous system and thus  
20 minimizes side reactions with lithium species located inside the carbon particle.

21  
22 As the constant current (CC) experiments exhibit a high capacity slightly below 0 V in the plateau  
23 region, we assumed a thermodynamically favoured formation of lithium species inside the carbon.  
24 Hence, we conducted a constant voltage measurement (ConVol) in which the half-cells were lithiated  
25 until 0 V, and subsequently a constant voltage of 0 V was applied until the current exceeds  $-7.5 \mu\text{A cm}^{-2}$   
26 (Figure 3). According to our understanding, bulk lithium metal should not deposit under these conditions  
27 since a certain overvoltage is normally required for plating. The resulting voltage profiles show a sloping  
28 region and continue with a plateau at the cut-off voltage of 0 V during discharge. The sloping and plateau  
29 capacities were separated at a potential of 20 mV to examine the differences between HC- and HCmicro-  
30 electrode (Figure 3c). The obtained capacities of the sloping region are quite comparable with slightly  
31 higher values close to  $150 \text{ mAh g}^{-1}_{\text{HC}}$  for the HC half-cell. However, the plateau capacities show a

1 remarkable difference with values of 108 to 92 mAh g<sup>-1</sup><sub>HC</sub> for HC and 457 to 330 mAh g<sup>-1</sup><sub>HCmicro</sub> for  
 2 HCmicro half-cells. As the plateau capacity at 0 V in the delithiation of HCs was assigned to lithium  
 3 insertion into microporous structure by Stevens and Dahn,<sup>42</sup> we can presume that our measured capacity  
 4 for the HCmicro-electrode results from lithium species forming inside the micropores. There are two  
 5 possible lithium species known from literature forming at potentials near and slightly below 0 V –  
 6 lithium clusters and lithium metal.<sup>23,31</sup>  
 7 For the interpretation of the ConVol measurements, it is important to state that the minimum potential  
 8 of the cell in constant voltage step was at -0.5 mV slightly below the intended 0 V due to the precision  
 9 of the measurement device. However, this is at least one order of magnitude smaller than the  
 10 overpotential for lithium metal plating observed in CC experiments e.g. for Li-Ni-foil cell and Li-Li  
 11 symmetric cell (Supplementary Figure 2). Therein the minimum of the potential dip attributed to the  
 12 beginning of lithium metal plating was located at values of -64.0 mV and -5.0 mV, respectively.  
 13 Additionally, the delithiation profile of the cells has only one plateau region at potentials between 0.02  
 14 and 0.2 V corresponding to the higher potential plateau in CC measurements. The first plateau below  
 15 0.02 V, previously assigned to the stripping of lithium metal, is missing. This suggests that no lithium  
 16 metal plating occurs in these experiments. In contrast, it shows the high capacity-gain by another lithium  
 17 form different from sloping capacity or formation of graphite intercalation compounds (GICs) like LiC<sub>6</sub>  
 18 (both above 0 V), and higher than cluster formation in hard carbons. In the 3<sup>rd</sup> charging cycle the  
 19 HCmicro cell exhibits a short circuit due to dendrite formation caused by the lithium metal counter  
 20 electrode. However, this has no influence on its previous performance and can be easily prevented by  
 21 using less dendrite-prone counter electrodes than lithium metal, e.g., a lithium-indium alloy. The  
 22 conducted cyclovoltammetry (CV) measurements on the HCmicro half-cell (see Supplementary  
 23 Figure 3) confirm that no plating of lithium metal occurs at potentials above and at -5 mV as they do  
 24 not comprise the classical plating/stripping peaks as visible in Li-Ni-foil cell cyclovoltammetry  
 25 (Supplementary Figure 3) or shown by Bonino et al.<sup>43</sup>

26  
27



28  
29 **Figure 3: Electrochemical characterization via constant voltage (ConVol) measurement.**  
 30 Galvanostatic measurements including a constant voltage step at 0 V during discharge until a cut-off  
 31 current of -7.5 μA cm<sup>-2</sup> for HCmicro (a) and HC (b) half-cells vs. lithium metal with constant current  
 32 (CC, hatched area) and constant voltage (CV) regions of the discharge/lithiation voltage profiles



1 separated by dotted lines in (a) and (b). (c) The corresponding capacities for sloping (until 20 mV, filled  
2 area) and plateau (below 20 mV, hatched area) region gathered from the discharge voltage profiles for  
3 HC (black) and HCmicro (red).

4  
5 In summary, the carbide derived carbon anode material (HCmicro) exhibits major advantages in half-  
6 cell performance comprising plateau capacity near 0 V vs. Li/Li<sup>+</sup>, high CE and delithiation capacity.  
7 HCmicro did not undergo any short-circuiting despite the fact that a high loading of 2.5 mAh cm<sup>-2</sup> was  
8 cycled and the measurements were performed at room temperature. To fully understand and explain the  
9 mechanism for this high plateau capacity, further investigations were conducted via NMR spectroscopy  
10 and SAXS measurements.

### 11 12 13 **<sup>7</sup>Li NMR spectroscopy studies of lithiated electrode materials**

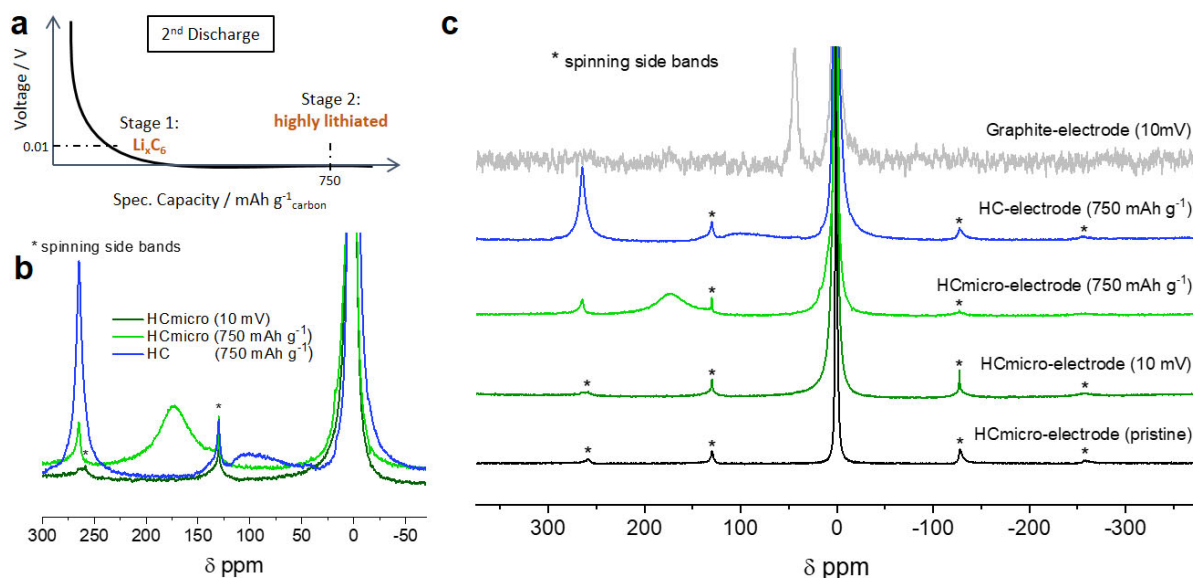
14 Magic angle spinning <sup>7</sup>Li nuclear magnetic resonance (<sup>7</sup>Li MAS NMR) spectra were measured ex-situ  
15 for varying stages of lithiation of graphite-, HC- and HCmicro-electrode to obtain further information  
16 about the evolving lithium structures and lithiation mechanism in the described cell system (Figure 4).  
17 Therefore, half-cells comprising the particular batch powders were pre-cycled once between 0.01 and  
18 2 V and afterwards discharged (lithiation of active material) until a certain cut-off criterion. The chosen  
19 cut-off criteria were defined as 10 mV (stage 1), the typical lithium intercalation cut-off for graphite  
20 anodes, and 750 mAh g<sup>-1</sup><sub>carbon</sub> (stage 2), for investigation of lithium species at highly lithiated stage  
21 (Figure 4a). To investigate the influence of lithium contained in the SE, the NMR spectrum was also  
22 measured on the pristine HCmicro-electrode. The resulting spectrum (Figure 4c) displays one intense  
23 signal at 1 ppm with spinning side bands of first and second order marked with asterisks (\*) in the  
24 diagram. Signals with very low chemical shift against the reference LiCl arise from ionic lithium species.  
25 Hence, the signal is attributed to lithium in the Li<sub>6</sub>PS<sub>5</sub>Cl argyrodite-type electrolyte.<sup>19,31</sup>

26  
27 The graphite-electrode material cycled to stage 1 (10 mV) was investigated to gain information about  
28 the solid-state <sup>7</sup>Li MAS NMR signal of intercalated lithium. In addition to the electrolyte signal at  
29 1 ppm, the spectrum exhibits a peak at 48 ppm as expected from literature revealing full lithiation to the  
30 graphite intercalation compound (GIC) stage I (LiC<sub>6</sub>).<sup>44-46</sup>

31 The HCmicro-electrode lithiated until 10 mV did not develop any signal apart from the electrolyte  
32 signal, which becomes slightly broadened compared with the pristine HCmicro-electrode. GICs with  
33 lower lithium content like diluted stages III and IV<sup>46</sup> are located at low chemical shift in NMR and  
34 therefore might overlap with the intense solid electrolyte peak at 1 ppm.<sup>45,47</sup> The formation of GIC stage  
35 I (LiC<sub>6</sub>) in HCmicro is unlikely due to the low density of perfect graphitic domains observed in TEM  
36 (see Figure 1). This explains the absence of the NMR peak at 48 ppm.

1 At 750 mAh g<sup>-1</sup><sub>HC</sub> lithiation (stage 2) of the HC-electrode a very broad signal starting from  
 2 approximately 35 ppm with its maximum at 105 ppm and almost reaching the first spinning side band  
 3 of the electrolyte peak at 130 ppm occurs (Figure 4b and c). Besides the electrolyte peak also another  
 4 signal at 263 ppm was observed. This signal can be assigned to metallic lithium deposited in the  
 5 electrode powder according to literature.<sup>23,34,48</sup> The broad signal around 105 ppm falls into the range  
 6 between intercalation signals from 0-50 ppm and the lithium metal at 263 ppm. According to literature  
 7 we therefore assign it to lithium clusters in the HC material.<sup>23,32,34,44,49</sup>  
 8 The HCmicro-electrode lithiated to stage 2 (750 mAh g<sup>-1</sup><sub>HCmicro</sub>) exhibits a distinct broad signal centered  
 9 at 175 ppm chemical shift. Further the signal at 263 ppm beforehand assigned to formation of lithium  
 10 metal in the electrode powder occurs in addition to the electrolyte peak at 1 ppm. The metallic lithium  
 11 signal is less intense for the HCmicro-electrode at stage 2 compared to the signal in the HC-electrode  
 12 (Figure 4b). This hints to a smaller amount of lithium metal in the HCmicro-electrode as the integral in  
 13 NMR corresponds to the number of associated nuclei at comparable sample weight. The short-circuit  
 14 observed in electrochemical cycling of the HC half-cells in contrast to the HCmicro half-cells supports  
 15 this observation (Figure 2b). The signal of the HCmicro-electrode at 175 ppm could not be assigned to  
 16 any chemical shift in room temperature <sup>7</sup>Li NMR spectra for disordered carbon electrodes known from  
 17 literature.<sup>23,32,34,49</sup> However, it also falls into the range of chemical shift predicted for lithium clusters  
 18 between 50 and 263 ppm.<sup>44</sup>

19  
 20



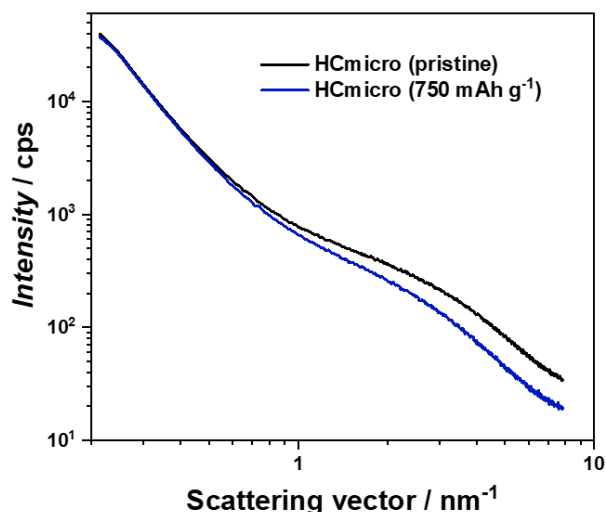
21  
 22 **Figure 4: <sup>7</sup>Li NMR spectroscopy at different lithiation degree.** Schematic voltage profile of the half-  
 23 cells in preparation for NMR measurement displaying second discharge with different cut-off stages for  
 24 cell disassembly (a). Room-temperature <sup>7</sup>Li MAS NMR spectra are shown with enlarged spectra of  
 25 HCmicro-electrode at stages 1 and 2 and HC-electrode at stage 2 for detailed signal comparison (b). The  
 26 full spectra of the different samples as described above are provided in (c). Spinning side bands are  
 27 denoted by asterisks (\*).

1  
2 A number of research groups have studied lithium cluster formation in HCs in combination with liquid  
3 electrolytes observing  $^7\text{Li}$  NMR signals at chemical shifts between 50 ppm and 120 ppm at room  
4 temperature.<sup>23,32,34,49</sup> The relatively high chemical shift of 175 ppm observed for the lithiated HCmicro-  
5 electrode is therefore rather unusual compared to literature-known HC cluster-signals and the herein  
6 described HC-electrode measurements. There are two different possibilities to explain the observed  
7 phenomenon. The first one is a higher free electron content in the clusters, which results in a Knight  
8 shift of the signal due to deshielding of the lithium nuclei.<sup>44</sup> This can occur due to a larger cluster size  
9 and would lead to a higher chemical shift of the  $^7\text{Li}$  NMR signal. In terms of conductivity, increasingly  
10 large clusters become more and more metallic. This results in effective chemical shifts closer to the  
11 signal of lithium metal than to the GIC peak.<sup>44</sup> The second possible explanation originates from the low  
12 graphitic structure of HCmicro. According to Tatsumi et al., the chemical shift of lithium clusters formed  
13 in HC is determined by the chemical exchange between clusters in microcavities and GICs. It is  
14 consequently moved to lower chemical shifts at room temperature while it splits into two peaks  
15 at  $-30\text{ }^\circ\text{C}$ .<sup>22,33,34</sup> The cluster signal for HC pore filling at temperatures below  $-30\text{ }^\circ\text{C}$  can be found at a  
16 chemical shift of approximately 180 ppm, which is in good agreement with the chemical shift of the  
17 herein depicted  $^7\text{Li}$  NMR signal at room temperature. Lithiated HCmicro might lack this shift due to the  
18 minor content of ordered graphite domains, which was pointed out earlier by TEM measurements.  
19 Further low temperature NMR measurements are required at this point to undoubtedly explain the  
20 observed signal. However, it can be concluded that lithium clusters exist in the lithiated HCmicro  
21 material, and that the lithium formation inside the HCmicro-electrode differs from the configuration in  
22 HCs.

23

#### 24 **Small Angle X-ray Scattering (SAXS) of lithiated HCmicro**

25 Further investigation on the HCmicro-electrode powder via SAXS measurement in sealed capillaries  
26 revealed a change of the scattering profile before and after lithiation (Figure 5). Therefore, the HCmicro-  
27 electrode was measured in the pristine and the lithiated stage discharged until  $750\text{ mAh g}^{-1}_{\text{HCmicro}}$  after  
28 pre-cycling with one initial formation cycle between 0.01 and 2 V. The obtained scattering profiles show  
29 a lowered intensity between 1 and  $8\text{ nm}^{-1}$  scattering vector for the lithiated HCmicro-electrode, which  
30 implies lower contribution of the scattering of single and aggregated micropores to the overall scattering.  
31 The difference in scattering intensity is also confirmed by measurements at various spots of the samples  
32 revealing identical scattering. This indicates a loss in microporosity due to lithium insertion inside the  
33 pores. A corresponding insertion mechanism has been described by Stevens et al. for lithium insertion  
34 in hard carbon material.<sup>42</sup>



1  
2 **Figure 5: SAXS analysis of HCmicro.** SAXS profiles of pristine (black) and lithiated HCmicro-  
3 electrode (blue) after pre-cycling in a half-cell vs. lithium metal between 0.01 and 2 V with a lithiation  
4 capacity of 750 mAh g<sup>-1</sup><sub>HCmicro</sub>.

5  
6 Based on these findings we can assume that the lithium gathers inside the microporosity of the HCmicro  
7 during electrochemical lithiation. We therefore propose a unique lithiation mechanism for HCmicro in  
8 all solid-state batteries as follows (Figure 6).

9  
10 **Proposal for lithium insertion mechanism**

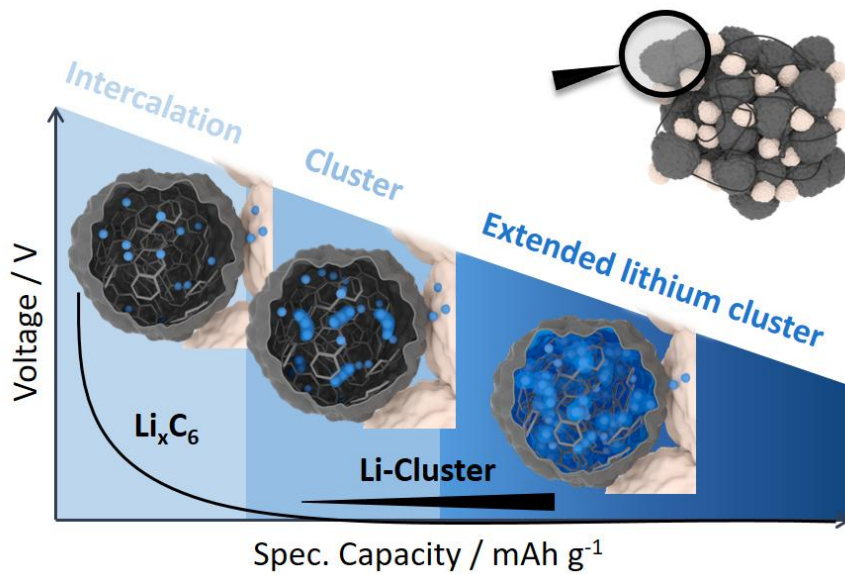
11 The second plateau observed in the delithiation step of both carbons in the constant current and the  
12 constant voltage experiments is a unique observation for the HCmicro, which shows no plateau capacity  
13 in liquid-electrolyte experiments.<sup>8,50</sup> A theoretical study on a graphene hetero structure with large  
14 interlayer distance by Bijoy and Murugan predicted the stabilization of extended lithium clusters  
15 between the layers with a slightly expanded interlayer distance of 3.4 Å.<sup>51</sup> In combination with our  
16 studies, this suggests the existence of such lithium clusters stabilized between the pore walls of  
17 HCmicro. The spatial pore-pore connection in HCmicro furthermore leads to connected pore voids and  
18 enables the formation of extended lithium clusters and advanced lithium storage compared to HC  
19 although comparable results concerning the size of micropores for both carbons were obtained in SAXS  
20 measurements. In larger pores, more clusters can combine. Thereby, they also eventually gain  
21 characteristics of bulk lithium, which is suggested by the existence of a short linear plateau at the  
22 beginning of the delithiation step and by the bulk lithium signal in <sup>7</sup>Li NMR despite the missing of a  
23 typical plating dip in the voltage profiles of the HCmicro.

24 Hence, we assign the second plateau of the electrochemical investigation of the half-cells to the  
25 delithiation of lithium clusters inside the porosity of the carbons. The higher capacity reached in this  
26 region for HCmicro-electrode compared to the HC-electrode gives further evidence for a higher amount  
27 of lithium nuclei assembled in its cluster structures as concluded from <sup>7</sup>Li MAS NMR measurements.  
28 Consequently, we propose that the formation of extended lithium clusters in the pore-pore connected,

1 accessible microporous system of the HCmicro is facilitated by the combination with the herein  
2 employed solid-state electrolyte.

3

4 In summary, the following mechanism for lithium insertion into HCmicro in an all solid-state set-up is  
5 proposed (Figure 6). As established in literature for hard carbons, the lithium ions firstly adsorb on  
6 defects or edges of the carbon surface in the sloping region of the potential curve. In the following  
7 potential plateau intercalation of  $\text{Li}^+$  in the small graphite-like domains of the HCmicro takes place.<sup>52</sup>  
8 Subsequently, lithium ions deposited at the edge of graphite-like domains and on pore walls start to form  
9 clusters which will extend in size upon further lithiation.<sup>24,53</sup> At a certain point, the growth of lithium  
10 metal will take place either when cluster size reaches high numbers of nuclei resulting in rearrangement,  
11 or eventually, the lithium may even start plating on the outer shell of the carbon when the porosity is  
12 completely filled. However, lithium metal formation occurs very homogeneous and no short-circuits  
13 were observed for HCmicro-electrode since there is a smooth transition from cluster to bulk lithium. We  
14 therefore name the herein presented approach a carbon/lithium hybrid anode-concept.



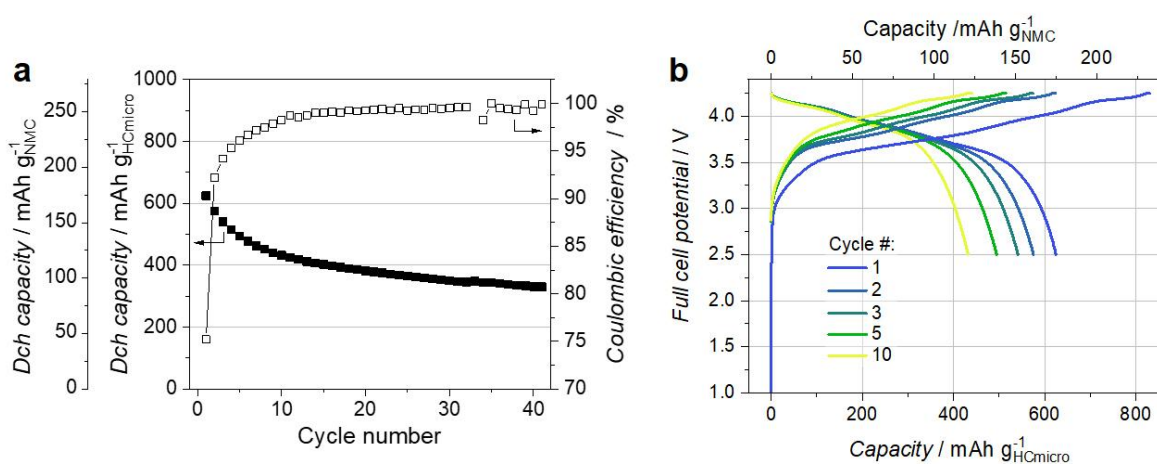
15  
16 **Figure 6: Proposed mechanism of lithium insertion in microporous carbon as anode material in**  
17 **all solid-state batteries.** Scheme divided into 3 phases: the intercalation of lithium, cluster formation  
18 as known from hard carbon lithiation and the formation of extended lithium clusters as special feature  
19 of the HCmicro anode material in all-solid-state electrolyte.

20  
21

### 22 Stable full-cell performance vs. NMC cathode

23 The excellent performance of the half-cells motivated us to demonstrate the first full-cell results  
24 combining the described carbon anode concept with a suitable cathode material (Figure 7 and  
25 Supplementary Figure 4). The full-cells consisting of a HCmicro-electrode anode and a nickel-rich  
26 NMC ( $\text{LiNi}_{0.9}\text{Mn}_{0.05}\text{Co}_{0.05}\text{O}_2$ ) cathode with  $\text{Li}_6\text{PS}_5\text{Cl}$  electrolyte exhibit relatively stable reversible

1 cycling performance over 40 cycles with coulombic efficiencies exceeding 98% in 10<sup>th</sup> cycle and at least  
 2 75% initial CE. The capacity of the cells starts with 174 mAh g<sup>-1</sup><sub>NMC</sub> concluding with 92 mAh g<sup>-1</sup><sub>NMC</sub> in  
 3 40<sup>th</sup> cycle. Based on the weight of the anode active material, this capacity results in 625 mAh g<sup>-1</sup><sub>HCmicro</sub>  
 4 for the 1<sup>st</sup> cycle. The average voltage was calculated via the measured energy and capacity values of  
 5 specific cycle step of the cell with 3.76 V in first discharge improving to 3.79 V in 10<sup>th</sup> cycle and  
 6 continuing at this value until 40<sup>th</sup> cycle (see Supplementary Note 1). This is a clear improvement  
 7 compared to the average voltage of 3.55 V in first discharge for a HC-electrode full-cell with comparable  
 8 composition continued with 3.53 V for 3<sup>rd</sup> discharge (see Supplementary Figure 4). It should be  
 9 mentioned that these results are the very first experiments on highly microporous carbons with reversible  
 10 capacity as high as 1000 mAh g<sup>-1</sup><sub>carbon</sub> in combination with argyrodite-type solid electrolyte and with a  
 11 nickel-rich cathode. Especially, these electrodes were assembled without any pre-lithiation of the carbon  
 12 anode or other additional lithium content. Therefore, all of the lithium capacity derives from the dry film  
 13 NMC cathode<sup>54</sup> and there is no additional lithium to replace irreversibly reacted lithium from side  
 14 reactions in the first cycles. As a consequence, these results underline the reversible (de)lithiation  
 15 concept of the HCmicro anode. So far, no further optimization was conducted regarding the balancing  
 16 of electrodes, the particle size and shape of the carbon or other commonly used procedures for  
 17 commercial battery improvement. Consequently, these results are of high value and are expected to be  
 18 further improved, e.g., by pre-lithiation of the carbon via chemical or physical approaches.<sup>55,56</sup>  
 19 Theoretical calculation of the investigated ASSB cell revealed projected gravimetric and volumetric  
 20 energy densities of 443 Wh kg<sup>-1</sup> and 1001 Wh L<sup>-1</sup> for the complete cell stack at n/p = 1 as utilized in the  
 21 experiment assuming an SE layer thickness of 30 μm (detailed calculation see Supplementary Table 1  
 22 and 2 plus Notes).



24  
 25 **Figure 7: Electrochemical characterization in full-cells.** Discharge (Dch) capacities calculated based  
 26 on HCmicro (anode) and NMC content (cathode) and coulombic efficiency of HCmicro/NMC all solid-  
 27 state full-cell (a) as well as voltage profiles of the first cycles shown in capacity per NMC (upper axis)  
 28 and per HCmicro (lower axis) (b).

29  
 30



## 1 **Conclusion**

2 Summarizing our findings, we were able to show a carbon/lithium hybrid anode-concept based on the  
3 microporous carbon anode material TiC-CDC (HCmicro) in an all solid-state battery to obtain high and,  
4 above all, reversible lithiation capacities of  $1000 \text{ mAh g}^{-1}_{\text{HCmicro}}$  with initial CE as high as 70% in half-  
5 cells.

6 The advancement regarding the cell concept presented herein is the long plateau region in the potential  
7 profile of the half-cell measurements at very low potential vs.  $\text{Li/Li}^+$ , which is a desired characteristic  
8 in order to significantly enhance full-cell energy density. Our investigations of the lithiation mechanism  
9 revealed the formation of lithium clusters inside the open pore system of HCmicro by  $^7\text{Li}$  MAS NMR  
10 cluster signal and gave evidence for a distinct lithium formation mechanism compared to hard carbon  
11 lithium clusters indicated by the characteristic chemical shift of the formed species. The unique  
12 combination of a porous carbon with the solid electrolyte enables the storage of highly dispersed and  
13 stabilized quasi-metallic lithium, which results in a highly reversible cell performance at room  
14 temperature. Finally, such a hybrid lithium-HCmicro anode concept was successfully combined and  
15 cycled 40 times vs. a nickel-rich NMC cathode. Without any extra lithium source beside the NMC  
16 cathode material, these full-cells obtained  $174 \text{ mAh g}^{-1}_{\text{NMC}}$  in 1<sup>st</sup> discharge and more than half of the  
17 initial capacity remained in 40<sup>th</sup> cycle. The average full-cell potential improved significantly compared  
18 with the HC full-cell by more than 0.2 V to a value of 3.76 V for the HCmicro full-cell, which leads to  
19 a projected energy density as high as  $443 \text{ Wh kg}^{-1}$ .

20 This work demonstrates the potential of porous carbons as 3-dimensional framework architectures for  
21 the stabilization of metallic or cluster-type lithium. The possibility to tune pore size, pore volume and  
22 pore functionalization of carbon materials and their combination with solid electrolytes is a promising  
23 option for the production of high capacity anodes for future high energy density prototype cells.

24

## 25 **Methods**

### 26 *Materials*

27 The carbon materials used for electrode preparation – hard carbon (HC, Kuraray Co., Ltd.), carbide-  
28 derived carbon (TiC-CDC-1000, HCmicro) and graphite powder – were dried for 12 h at  $200 \text{ }^\circ\text{C}$  under  
29 vacuum before use. The TiC-CDC-1000 (HCmicro) was synthesized at Technical University Dresden  
30 from TiC particles (Sigma Aldrich, -325 mesh, 98%) via chlorination process at  $1000 \text{ }^\circ\text{C}$  as previously  
31 described by Borchardt et al.<sup>57</sup> Argyrodite type solid electrolyte ( $\text{Li}_6\text{PS}_5\text{Cl}$ , SE) with approx.  $3 \text{ }\mu\text{m}$  and  
32  $15 \text{ }\mu\text{m}$  particle diameter was utilized as received for electrode batch preparation and SE pellet in cell  
33 stacks, respectively. Lithium metal foil was purchased with a thickness of  $50 \text{ }\mu\text{m}$  from China Energy  
34 Lithium Co., Ltd. and was prepared in an Ar-filled glove box via punching out disks with  $13 \text{ mm}$   
35 diameter.  $\text{Li}_2\text{O-ZrO}_2$  (LZO) coated  $\text{LiNi}_{0.9}\text{Co}_{0.05}\text{Mn}_{0.05}\text{O}_2$  (NMC) was prepared by the sol-gel method  
36 based on  $\text{ZrO}_2$  coating as stated in a previous publication.<sup>54</sup>

1 All further material handling and cell preparation was conducted under inert gas atmosphere in an Ar-  
2 filled glovebox with moisture and air content below 0.01 ppm.

3

#### 4 *Electrode materials preparation*

5 To prepare the anode composite electrode powders further named as HCmicro-, HC- and graphite-  
6 electrode, the dried carbon - HCmicro, HC and graphite, respectively - was mixed manually with  
7 conductive carbon additive (CNF, CNF\_PR-25-XT-HHT, Pyrograf), and SE (Li<sub>6</sub>PS<sub>5</sub>Cl, 3 μm particle  
8 diameter) in the mass ratio of 60:5:35 for 30 min in an agate mortar.

9 NMC-cathodes for full-cell experiments were prepared via dry-film processing as described by Hippauf  
10 et al.<sup>54</sup> with 16.1 mg<sub>AM</sub>/cm<sup>2</sup> loading of LZO-coated NMC with a mass ratio of 85:2:13 of NMC:CNF:SE.

11

#### 12 *Half-cell and full-cell preparation*

13 The half-cells were prepared in a stainless steel outer casing with a polyoxymethylene liner by using a  
14 die with a diameter of 13 mm. Therefore, a lithium foil with a diameter of 13 mm and 50 μm thickness  
15 was arranged inside the die and SE powder (150 mg ±0.5 mg) was uniformly spread on top by a micro-  
16 spatula. This composition was temporarily compressed and compacted into a pellet. Afterwards, the  
17 composite powder HCmicro-, HC- or graphite-electrode, respectively, (7.37 mg ±0.2 mg) was  
18 homogeneously distributed across the compacted electrolyte surface in the die and again compressed by  
19 using a hydraulic press applying 4 tons for 30 s. The resulting areal active material loading of the half-  
20 cell was 3.33 mg cm<sup>-2</sup>. Before cell performance measurement, the cells were closed airtight inside a  
21 pouch bag.

22 Full cells were prepared similar to half-cell preparation except for the lithium foil, which was replaced  
23 by the NMC-cathode and was positioned centered on top of the SE pellet after the carbon-anode  
24 preparation and the SE pellet formation.

25

#### 26 *Electrochemical measurements*

27 All cells were stored for 5 hours after assembly before electrochemical measurement started. The cell  
28 performance measurements were conducted on a battery tester CTS-Lab (BaSyTec, Germany). The half-  
29 cells were discharged with 0.05 mA cm<sup>-2</sup> until a constant capacity of 1000 mAh g<sup>-1</sup> or cut off if going  
30 below -0.02 V earlier followed by a 30-min-pause and a subsequent charging at the same areal current  
31 density until 2 V. This procedure was repeated for 10 cycles.

32 The full-cells were cycled between 2.5 and 4.25 V with a constant voltage step at the end of each  
33 charging until a cut-off current of 0.015 mA cm<sup>-2</sup>. The areal current density was 0.05 mA cm<sup>-2</sup> as well.

34 Further electrochemical experiments were conducted on a VSP-300 (Bio-Logic, France). Constant  
35 voltage measurements (ConVol) were conducted with pre-cycling between 0.01 and 2 V with a current  
36 density of 0.05 mA cm<sup>-2</sup> for 2 times. A constant current (CC) step in discharge with 0.05 mA cm<sup>-2</sup> until

1 0 V and subsequent ConVol step at 0 V until a cut-off current of  $-7.5 \mu\text{A cm}^{-2}$  followed for 3 cycles with  
2 in between charging at  $0.05 \text{ mA cm}^{-2}$  to 2 V.

3 Cyclovoltammetry (CV) procedure was conducted with  $0.01 \text{ mV s}^{-1}$  between the upper cut-off voltage  
4 at 1 V and changing lower cut-off voltages of 10, 2, 0 and -5 mV each for 4 cycles. The I-step duration  
5 was set to 50%.

6

### 7 *Materials characterization*

8 Powder X-ray diffraction (XRD) patterns were measured on a Bruker D8 in Bragg-Brentano geometry  
9 in a  $2\Theta$  range of  $10\text{-}70^\circ$  with a resolution of  $0.03^\circ$  using  $\text{CuK}\alpha$  radiation ( $\lambda=0.15418 \text{ nm}$ ) and a NaI  
10 scintillation detector. The samples were placed on a horizontal silicon single crystal holder.

11 Nitrogen physisorption isotherms were measured via low-pressure nitrogen physisorption at 77 K with  
12 an Autosorb 1C apparatus (Quantachrome), using 10-20 mg of activated sample. Activation was  
13 conducted under vacuum for 12 h at  $200^\circ\text{C}$  after a heating period of 2 h on a Belprep Vac II. The  
14 multipoint BET equation ( $p/p_0 = 0.05\text{-}0.2$ ) served for calculation of the specific surface area, whereas  
15 pore volumes were estimated from the volume of adsorbed nitrogen at  $p/p_0 = 0.97$  for the micro- and  
16 mesoporous content. The quenched-solid density functional theory (QSDFT) for nitrogen at 77 K on  
17 carbon with slit/cylindrical pores (adsorption branch) was utilized to retrieve the pore size distributions  
18 (PSDs).

19 For Raman measurements, a Renishaw inVia microscope with an excitation laser wavelength of 514 nm  
20 at 5% laser power ( $0.1 \text{ mW } \mu\text{m}^{-3}$ ) and 50-fold magnification was used measuring between 100 and  
21  $3500 \text{ cm}^{-1}$  for two times 30 s. The intensity ratio  $I(\text{D})/I(\text{G})$  was calculated from the fitting of G-Peak via  
22 Breit-Wigner-Fano and D-Peak with Lorentz fitting with a linear base line analysed from  $1200 \text{ cm}^{-1}$  to  
23  $1750 \text{ cm}^{-1}$ .

24 Small-angle X-ray scattering was measured on a Bruker Nanostar 2 device using  $\text{CuK}\alpha$  radiation in  
25 transmission geometry with 279 mm distance between sample and detector at a vacuum level of  
26 approximately 0.02 mbar. Prior to each measurement, samples were filled into borosilicate capillaries  
27 inside the glovebox, temporarily closed with polymer foil and finally sealed by melting the glass,  
28 immediately after extraction from the glovebox.

29 Solid-state  $^7\text{Li}$  MAS NMR experiments were carried out on a BRUKER Avance NEO 300 MHz  
30 spectrometer at a resonance frequency of 116.6 MHz with a commercial double resonance 2.5 MAS  
31 NMR probe operating at a MAS frequency of 15 kHz. 32 Scans were accumulated. The pulse repetition  
32 time was 60 s. SPINAL 1H-decoupling was applied during signal acquisition. The lithium chemical shift  
33 was referenced with LiCl.

34 The TEM investigations were conducted using a double-Cs-corrected Jeol ARM200F, equipped with a  
35 cold field emission gun and operated with an acceleration voltage of 80 kV as well as on a TEM JEM-  
36 211, JEOL.

1 Scanning electron microscopy (SEM) was performed on a HITACHI SU8020 at 2.0 kV with a working  
2 distance of 8.9 and 15.3 mm for HC and HCmicro, respectively. The samples were sputtered on a Q150R  
3 ES (Quorum) with Au nanoparticles ( $\leq 10$  nm) before SEM measurement.  
4

## 5 **References**

- 6 1. Wu, F., Maier, J. & Yu, Y. Guidelines and trends for next-generation rechargeable lithium and  
7 lithium-ion batteries. *Chemical Society reviews* **49**, 1569–1614; 10.1039/C7CS00863E (2020).
- 8 2. Lin, D., Liu, Y. & Cui, Y. Reviving the lithium metal anode for high-energy batteries. *Nature*  
9 *nanotechnology* **12**, 194–206; 10.1038/NNANO.2017.16 (2017).
- 10 3. Li, L., Li, S. & Lu, Y. Suppression of dendritic lithium growth in lithium metal-based batteries.  
11 *Chemical communications* **54**, 6648–6661; 10.1039/c8cc02280a (2018).
- 12 4. Cheng, X.-B., Zhang, R., Zhao, C.-Z. & Zhang, Q. Toward Safe Lithium Metal Anode in  
13 Rechargeable Batteries: A Review. *Chemical reviews* **117**, 10403–10473;  
14 10.1021/acs.chemrev.7b00115 (2017).
- 15 5. Xu, B. *et al.* Nano-CaCO<sub>3</sub> templated mesoporous carbon as anode material for Li-ion batteries.  
16 *Electrochimica Acta* **56**, 6464–6468; 10.1016/j.electacta.2011.04.130 (2011).
- 17 6. Velez, V. *et al.* Synthesis of novel hard mesoporous carbons and their applications as anodes for Li  
18 and Na ion batteries. *Carbon* **147**, 214–226; 10.1016/j.carbon.2019.02.083 (2019).
- 19 7. Kubota, K. *et al.* Structural Analysis of Sucrose-Derived Hard Carbon and Correlation with the  
20 Electrochemical Properties for Lithium, Sodium, and Potassium Insertion. *Chem. Mater.*;  
21 10.1021/acs.chemmater.9b05235 (2020).
- 22 8. Sakamoto, K. M. Master's Thesis. Naval Postgraduate School, 2011/09.
- 23 9. Weber, R. *et al.* Long cycle life and dendrite-free lithium morphology in anode-free lithium pouch  
24 cells enabled by a dual-salt liquid electrolyte. *Nat Energy* **4**, 683–689; 10.1038/s41560-019-0428-9  
25 (2019).
- 26 10. Louli, A. J. *et al.* Exploring the Impact of Mechanical Pressure on the Performance of Anode-Free  
27 Lithium Metal Cells. *J. Electrochem. Soc.* **166**, A1291-A1299; 10.1149/2.0091908jes (2019).
- 28 11. Bai, P., Li, J., Brushett, F. R. & Bazant, M. Z. Transition of lithium growth mechanisms in liquid  
29 electrolytes. *Energy Environ. Sci.* **9**, 3221–3229; 10.1039/C6EE01674J (2016).
- 30 12. Cheng, X.-B. *et al.* A Review of Solid Electrolyte Interphases on Lithium Metal Anode. *Advanced*  
31 *science (Weinheim, Baden-Wurttemberg, Germany)* **3**, 1500213; 10.1002/advs.201500213 (2016).
- 32 13. Zhao, C.-Z. *et al.* Designing solid-state interfaces on lithium-metal anodes: a review. *Sci. China*  
33 *Chem.* **62**, 1286–1299; 10.1007/s11426-019-9519-9 (2019).
- 34 14. Shi, P. *et al.* A Review of Composite Lithium Metal Anode for Practical Applications. *Adv. Mater.*  
35 *Technol.* **5**, 1900806; 10.1002/admt.201900806 (2020).

- 1 15. Isaev, I. *et al.* A new approach for the preparation of anodes for Li-ion batteries based on activated  
2 hard carbon cloth with pore design. *Journal of Power Sources* **119-121**, 28–33; 10.1016/S0378-  
3 7753(03)00119-8 (2003).
- 4 16. Ye, W. *et al.* Stable Nano-Encapsulation of Lithium Through Seed-Free Selective Deposition for  
5 High-Performance Li Battery Anodes. *Adv. Energy Mater.* **10**, 1902956; 10.1002/aenm.201902956  
6 (2020).
- 7 17. Zheng, G. *et al.* Interconnected hollow carbon nanospheres for stable lithium metal anodes. *Nature*  
8 *nanotechnology* **9**, 618–623; 10.1038/NNANO.2014.152 (2014).
- 9 18. Hippauf, F. *et al.* The Importance of Pore Size and Surface Polarity for Polysulfide Adsorption in  
10 Lithium Sulfur Batteries. *Adv. Mater. Interfaces* **3**, 1600508; 10.1002/admi.201600508 (2016).
- 11 19. Oschatz, M. *et al.* (Elsevier2016), pp. 237–318.
- 12 20. Seitz, A. E., Hippauf, F., Kremer, W., Kaskel, S. & Scheer, M. Facile storage and release of white  
13 phosphorus and yellow arsenic. *Nature Communications* **9**, 361; 10.1038/s41467-017-02735-2  
14 (2018).
- 15 21. Sugano, S., Nishina, Y. & Ohnishi, S. *Microclusters. Proceedings of the First NEC Symposium,*  
16 *Hakone and Kawasaki, Japan, October 20-23, 1986* (Springer, Berlin, Heidelberg, 1987).
- 17 22. Tatsumi, K. *et al.*  $^7\text{Li}$  NMR studies on a lithiated non-graphitizable carbon fibre at low temperatures.  
18 *Chem. Commun.*, 687–688; 10.1039/A700221A (1997).
- 19 23. Gotoh, K. *et al.* Mechanisms for overcharging of carbon electrodes in lithium-ion/sodium-ion  
20 batteries analysed by operando solid-state NMR. *J. Mater. Chem. A* **8**, 14472–14481;  
21 10.1039/D0TA04005C (2020).
- 22 24. Morita, R. *et al.* Combination of solid state NMR and DFT calculation to elucidate the state of  
23 sodium in hard carbon electrodes. *J. Mater. Chem. A* **4**, 13183–13193; 10.1039/c6ta04273b (2016).
- 24 25. Gogotsi, Y. *et al.* Nanoporous carbide-derived carbon with tunable pore size. *Nature Materials* **2**,  
25 591–594; 10.1038/nmat957 (2003).
- 26 26. Chmiola, J., Yushin, G., Dash, R. & Gogotsi, Y. Effect of pore size and surface area of carbide  
27 derived carbons on specific capacitance. *Journal of Power Sources* **158**, 765–772;  
28 10.1016/j.jpowsour.2005.09.008 (2006).
- 29 27. Largeot, C. *et al.* Relation between the ion size and pore size for an electric double-layer capacitor.  
30 *Journal of the American Chemical Society* **130**, 2730–2731; 10.1021/ja7106178 (2008).
- 31 28. Presser, V., Heon, M. & Gogotsi, Y. Carbide-Derived Carbons - From Porous Networks to  
32 Nanotubes and Graphene. *Adv. Funct. Mater.* **21**, 810–833; 10.1002/adfm.201002094 (2011).
- 33 29. Letellier, M. in *Encyclopedia of Spectroscopy and Spectrometry* (Elsevier2017), pp. 181–191.
- 34 30. Letellier, M., Chevallier, F. & Morcrette, M. In situ  $^7\text{Li}$  nuclear magnetic resonance observation of  
35 the electrochemical intercalation of lithium in graphite; 1st cycle. *Carbon* **45**, 1025–1034;  
36 10.1016/j.carbon.2006.12.018 (2007).

- 1 31. Letellier, M. *et al.* The first in situ  $^7\text{Li}$  nuclear magnetic resonance study of lithium insertion in hard-  
2 carbon anode materials for Li-ion batteries. *The Journal of Chemical Physics* **118**, 6038–6045;  
3 10.1063/1.1556092 (2003).
- 4 32. Fujimoto, H., Mabuchi, A., Tokumitsu, K., Chinnasamy, N. & Kasuh, T.  $^7\text{Li}$  nuclear magnetic  
5 resonance studies of hard carbon and graphite/hard carbon hybrid anode for Li ion battery. *Journal*  
6 *of Power Sources* **196**, 1365–1370; 10.1016/j.jpowsour.2010.09.026 (2011).
- 7 33. Tatsumi, K. *et al.* Low temperature  $^7\text{Li}$ -NMR investigations on lithium inserted into carbon anodes  
8 for rechargeable lithium-ion cells. *Journal of Power Sources* **81-82**, 397–400; 10.1016/S0378-  
9 7753(99)00114-7 (1999).
- 10 34. Gotoh, K. *et al.* Properties of a novel hard-carbon optimized to large size Li ion secondary battery  
11 studied by  $^7\text{Li}$  NMR. *Journal of Power Sources* **162**, 1322–1328; 10.1016/j.jpowsour.2006.09.001  
12 (2006).
- 13 35. Qiu, S. *et al.* Manipulating Adsorption–Insertion Mechanisms in Nanostructured Carbon Materials  
14 for High-Efficiency Sodium Ion Storage // Manipulating Adsorption-Insertion Mechanisms in  
15 Nanostructured Carbon Materials for High-Efficiency Sodium Ion Storage. *Advanced Energy*  
16 *Materials* **7**, 1700403; 10.1002/aenm.201700403 (2017).
- 17 36. Dash, R. *et al.* Titanium carbide derived nanoporous carbon for energy-related applications. *Carbon*  
18 **44**, 2489–2497; 10.1016/j.carbon.2006.04.035 (2006).
- 19 37. Thommes, M. *et al.* Physisorption of gases, with special reference to the evaluation of surface area  
20 and pore size distribution (IUPAC Technical Report). *Pure and Applied Chemistry* **87**, 1051–1069;  
21 10.1515/pac-2014-1117 (2015).
- 22 38. Buiel, E., George, A. E. & Dahn, J. R. On the Reduction of Lithium Insertion Capacity in Hard-  
23 Carbon Anode Materials with Increasing Heat-Treatment Temperature. *J. Electrochem. Soc.* **145**,  
24 2252–2257; 10.1149/1.1838629 (1998).
- 25 39. Saurel, D. *et al.* A SAXS outlook on disordered carbonaceous materials for electrochemical energy  
26 storage. *Energy Storage Materials* **21**, 162–173; 10.1016/j.ensm.2019.05.007 (2019).
- 27 40. Yang, C.-P., Yin, Y.-X., Zhang, S.-F., Li, N.-W. & Guo, Y.-G. Accommodating lithium into 3D  
28 current collectors with a submicron skeleton towards long-life lithium metal anodes. *Nature*  
29 *Communications* **6**, 8058; 10.1038/ncomms9058 (2015).
- 30 41. Yang, G. *et al.* Insights into Lithium and Sodium Storage in Porous Carbon. *Nano Letters*;  
31 10.1021/acs.nanolett.0c00943 (2020).
- 32 42. Stevens, D. A. & Dahn, J. R. The Mechanisms of Lithium and Sodium Insertion in Carbon Materials.  
33 *J. Electrochem. Soc.* **148**, A803; 10.1149/1.1379565 (2001).
- 34 43. Bonino, F. A Polymeric Electrolyte Rechargeable Lithium Battery. *J. Electrochem. Soc.* **135**, 12–  
35 15; 10.1149/1.2095538 (1988).
- 36 44. Tatsumi, K. *et al.*  $^7\text{Li}$  -Nuclear Magnetic Resonance Observation of Lithium Insertion into  
37 Mesocarbon Microbeads. *J. Electrochem. Soc.* **143**, 1923–1930; 10.1149/1.1836926 (1996).



- 1 45. Chevallier, F., Poli, F., Montigny, B. & Letellier, M. In situ  $^7\text{Li}$  nuclear magnetic resonance  
2 observation of the electrochemical intercalation of lithium in graphite: second cycle analysis.  
3 *Carbon* **61**, 140–153; 10.1016/j.carbon.2013.04.078 (2013).
- 4 46. Boehm, H. P., Setton, R. & Stumpp, E. Nomenclature and terminology of graphite intercalation  
5 compounds (IUPAC Recommendations 1994). *Pure and Applied Chemistry* **66**, 1893–1901;  
6 10.1351/pac199466091893 (1994).
- 7 47. Zaghbi, K. *et al.*  $^7\text{Li}$  - NMR of Well-Graphitized Vapor-Grown Carbon Fibers and Natural Graphite  
8 Negative Electrodes of Rechargeable Lithium-Ion Batteries. *J. Electrochem. Soc.* **146**, 2784–2793;  
9 10.1149/1.1392009 (1999).
- 10 48. Weiss, A. G. S. Carter, L. H. Bennett, D. J. Kahan: Metallic Shifts in NMR, A review of theory and  
11 comprehensive critical data compilation of metallic materials. Part I-IV (Progress in Materials  
12 Science, Vol. 20, Editors: B. Chalmers, J. W. Christian, T. B. Massals. *Berichte der*  
13 *Bunsengesellschaft für physikalische Chemie* **81**, 779–780; 10.1002/bbpc.19770810824 (1977).
- 14 49. Chevallier, F. *et al.* In Situ  $^7\text{Li}$ -Nuclear Magnetic Resonance Observation of Reversible Lithium  
15 Insertion into Disordered Carbons. *Electrochemical and Solid-State Letters* **6**, A225;  
16 10.1149/1.1612011 (2003).
- 17 50. Yeon, S.-H., Jung, K.-N., Yoon, S., Shin, K.-H. & Jin, C.-S. Electrochemical performance of  
18 carbide-derived carbon anodes for lithium-ion batteries. *Journal of Physics and Chemistry of Solids*  
19 **74**, 1045–1055; 10.1016/j.jpcc.2013.02.028 (2013).
- 20 51. Bijoy, T. K. & Murugan, P. Lithiation of the Two-Dimensional Silicon Carbide–Graphene van der  
21 Waals Heterostructure: A First Principles Study. *J. Phys. Chem. C* **123**, 10738–10745;  
22 10.1021/acs.jpcc.8b12492 (2019).
- 23 52. Ghimbeu, C. M. *et al.* Insights on the  $\text{Na}^+$  ion storage mechanism in hard carbon: Discrimination  
24 between the porosity, surface functional groups and defects. *Nano Energy* **44**, 327–335;  
25 10.1016/j.nanoen.2017.12.013 (2018).
- 26 53. Kotina, I.M. *et al.* Study of the lithium diffusion in nanoporous carbon materials produced from  
27 carbides. *Journal of Non-Crystalline Solids* **299-302**, 815–819; 10.1016/S0022-3093(01)01124-3  
28 (2002).
- 29 54. Hippauf, F. *et al.* Overcoming binder limitations of sheet-type solid-state cathodes using a solvent-  
30 free dry-film approach. *Energy Storage Materials* **21**, 390–398; 10.1016/j.ensm.2019.05.033  
31 (2019).
- 32 55. Shen, Y., Qian, J., Yang, H., Zhong, F. & Ai, X. Chemically Pre-lithiated Hard-Carbon Anode for  
33 High Power and High Capacity Li-Ion Batteries. *Small (Weinheim an der Bergstrasse, Germany)*  
34 **16**, e1907602; 10.1002/sml.201907602 (2020).
- 35 56. Holtstiege, F., Schmuch, R., Winter, M., Bruncklaus, G. & Placke, T. New insights into pre-lithiation  
36 kinetics of graphite anodes via nuclear magnetic resonance spectroscopy. *Journal of Power Sources*  
37 **378**, 522–526; 10.1016/j.jpowsour.2017.12.069 (2018).

1 57. Borchardt, L., Oschatz, M., Paasch, S., Kaskel, S. & Brunner, E. Interaction of electrolyte molecules  
2 with carbon materials of well-defined porosity: characterization by solid-state NMR spectroscopy.  
3 *Physical chemistry chemical physics : PCCP* **15**, 15177–15184; 10.1039/c3cp52283k (2013).  
4

#### 5 **Acknowledgments**

6 This research is funded by the European Social Fund and co-financed by tax funds based on the budget  
7 approved by the members of the Saxon State Parliament. This work was supported by the Fraunhofer  
8 and Max Planck cooperation programme.

9 The authors are thankful to Daniel Werner (Max Planck Institute of Colloids and Interfaces, Potsdam)  
10 for conducting the SAXS measurements and to Dr. Tobias Heil (Max Planck Institute of Colloids and  
11 Interfaces, Potsdam) and Dr. Jörg Kaspar (Fraunhofer Institute IWS, Dresden) for performing the  
12 Transmission Electron Microscopy. Rene Zenner (Fraunhofer Institute IWS, Dresden) is acknowledged  
13 for designing and constructing the graphic for proposed cluster formation mechanism. The authors thank  
14 Susann Kleber (Fraunhofer Institute IWS, Dresden) for performing the Raman measurements.  
15

#### 16 **Author information:**

##### 17 *Affiliations:*

18 <sup>a</sup> Technical University Dresden, Chair of Inorganic Chemistry I, Bergstraße 66, 01069 Dresden,  
19 Germany

20 <sup>b</sup> Fraunhofer Institute for Material and Beam Technology IWS, Winterbergstr. 28, 01277 Dresden,  
21 Germany

22 <sup>c</sup> Technical University Dresden, Chair of Bioanalytical Chemistry, Bergstraße 66, 01069 Dresden,  
23 Germany

24 <sup>d</sup> Max Planck Institute of Colloids and Interfaces, Dept. of Colloid Chemistry, Am Mühlenberg 1, 14476  
25 Potsdam, Germany

26 <sup>e</sup> Friedrich-Schiller-University Jena, Institute for Technical Chemistry and Environmental Chemistry,  
27 Center for Energy and Environmental Chemistry Jena (CEEC Jena), Philosophenweg 7a, 07743, Jena,  
28 Germany  
29

##### 30 *Contributions:*

31 L. M. Bloi performed the battery experiments, designed NMR measurement preparation, analysed data  
32 and wrote the manuscript. F. Hippauf and T. Boenke assisted in conception of experiments and  
33 substantially edited the manuscript. M. Rauche and S. Paasch performed the <sup>7</sup>Li NMR measurements  
34 and assisted with the interpretation of the results. K. Schütjajew analysed the SAXS data and conducted  
35 the XRD experiments. F. Schwotzer performed all SEM measurements and assisted in interpretation of  
36 data. J. Pampel, S. Dörfler, H. Althues and M. Oschatz conceived the project and edited the manuscript.

1 S. Dörfler, H. Althues and M. Oschatz discussed the results and implications of the project. E. Brunner  
2 and S. Kaskel supervised the project and commented on the manuscript.

3

4 *Corresponding author:*

5 Correspondence to Stefan Kaskel (\*E-mail: stefan.kaskel@tu-dresden.de).

6

7 **Competing interests:**

8 The authors declare no competing financial or non-financial interests.

9

10 **Supplementary Information:**

11 Supplementary Tables 1-2, Figures 1-4, Notes and references.